

## A Precursory Signal of June/July Precipitation over the Yangtze River Basin: December/January Tropospheric Temperature over the Tibetan Plateau

Xiaying ZHU, Mingzhu YANG, Ge LIU, Yanju LIU, Weijing LI, Sulan NAN, Linhai SUN

**Citation:** Zhu, X. Y., M. Z. Yang, G. Liu, Y. J. Liu, W. J. Li, S. L. Nan, and L. H. Sun 2023: A Precursory Signal of June/July Precipitation over the Yangtze River Basin: December/January Tropospheric Temperature over the Tibetan Plateau, *Adv. Atmos. Sci.*, 40, 1986–1997. doi: [10.1007/s00376-022-2079-1](https://doi.org/10.1007/s00376-022-2079-1).

View online: <https://doi.org/10.1007/s00376-022-2079-1>

## Related articles that may interest you

[Subseasonal Change in the Seesaw Pattern of Precipitation between the Yangtze River Basin and the Tropical Western North Pacific during Summer](#)

Advances in Atmospheric Sciences. 2018, 35(10), 1231 <https://doi.org/10.1007/s00376-018-7304-6>

[Subseasonal and Synoptic Variabilities of Precipitation over the Yangtze River Basin in the Summer of 2020](#)

Advances in Atmospheric Sciences. 2021, 38(12), 2108 <https://doi.org/10.1007/s00376-021-1133-8>

[Toward Understanding the Extreme Floods over Yangtze River Valley in June/July 2020: Role of Tropical Oceans](#)

Advances in Atmospheric Sciences. 2021, 38(12), 2023 <https://doi.org/10.1007/s00376-021-1036-8>

[Attribution of Persistent Precipitation in the Yangtze–Huaihe River Basin during February 2019](#)

Advances in Atmospheric Sciences. 2020, 37(12), 1389 <https://doi.org/10.1007/s00376-020-0107-6>

[Morphological Characteristics of Precipitation Areas over the Tibetan Plateau Measured by TRMM PR](#)

Advances in Atmospheric Sciences. 2021, 38(4), 677 <https://doi.org/10.1007/s00376-020-0233-1>

[Sources of Subseasonal Prediction Skill for Heatwaves over the Yangtze River Basin Revealed from Three S2S Models](#)

Advances in Atmospheric Sciences. 2020, 37(12), 1435 <https://doi.org/10.1007/s00376-020-0144-1>



AAS Website



AAS Weibo



AAS WeChat

Follow AAS public account for more information

• Original Paper •

# A Precursory Signal of June–July Precipitation over the Yangtze River Basin: December–January Tropospheric Temperature over the Tibetan Plateau<sup>✱</sup>

Xiaying ZHU<sup>1</sup>, Mingzhu YANG<sup>1</sup>, Ge LIU<sup>\*2,3</sup>, Yanju LIU<sup>1</sup>, Weijing LI<sup>1</sup>, Sulan NAN<sup>2</sup>, and Linhai SUN<sup>1</sup>

<sup>1</sup>National Climate Center, Beijing 100081, China

<sup>2</sup>State Key Laboratory of Severe Weather, Chinese Academy of Meteorological Sciences, Beijing 100081, China

<sup>3</sup>Collaborative Innovation Centre on Forecast and Evaluation of Meteorological Disasters, Nanjing University of Information Science and Technology, Nanjing 210044, China

(Received 18 March 2022; revised 11 July 2022; accepted 4 August 2022)

## ABSTRACT

The prediction of summer precipitation over the Yangtze River basin (YRB) has long been challenging, especially during June–July (JJ), when the mei-yu generally occurs. This study explores the potential signal for the YRB precipitation in JJ and reveals that the Tibetan Plateau tropospheric temperature (TPTT) in the middle and upper levels during the preceding December–January (DJ) is significantly correlated with JJ YRB precipitation. The close connection between the DJ TPTT anomaly with JJ YRB precipitation may be due to the joint modulation of the DJ ENSO and spring TP soil temperatures. The lagged response to an anomalously cold TPTT during the preceding DJ is a TPTT that is still anomalously cold during the following JJ. The lower TPTT can lead to an anomalous anticyclone to the east of Lake Baikal, an anomalous cyclone at the middle latitudes of East Asia, and an anomalous anticyclone over the western North Pacific. Meanwhile, the East Asian westerly jet shifts southward in response to the meridional thermal gradient caused by the colder troposphere extending from the TP to the east of Lake Baikal. The above-mentioned circulation anomalies constitute the positive anomaly of the East Asia-Pacific pattern, known to be conducive to more precipitation over the YRB. Since the DJ TPTT contains both the land (TP soil temperature) and ocean (ENSO) signals, it has a closer relationship with the JJ precipitation over the YRB than the DJ ENSO alone. Therefore, the preceding DJ TPTT can be considered an alternative predictor of the JJ YRB precipitation.

**Key words:** Tibetan Plateau, thermal condition, Yangtze River, precipitation, prediction

**Citation:** Zhu, X. Y., M. Z. Yang, G. Liu, Y. J. Liu, W. J. Li, S. L. Nan, and L. H. Sun, 2023: A precursory signal of June–July precipitation over the Yangtze River Basin: December–January tropospheric temperature over the Tibetan Plateau. *Adv. Atmos. Sci.*, **40**(11), 1986–1997, <https://doi.org/10.1007/s00376-022-2079-1>.

## Article Highlights:

- December–January (DJ) Tibetan Plateau tropospheric temperature (TPTT) can be considered a predictor of June–July precipitation over the Yangtze River basin (YRB).
- A DJ TPTT anomaly can reflect the JJ TPTT well and cause an anomalous East Asia-Pacific pattern and associated precipitation over the YRB in JJ.
- A DJ TPTT contains both the land and oceanic signals and therefore has a closer relationship with the JJ precipitation over the YRB than ENSO.

## 1. Introduction

The East Asian summer monsoon (EASM) features an elongated rain belt from eastern China to Japan via Korea,

which is called mei-yu in China, Baiu in Japan, and Changma in Korea. The mei-yu generally appears over the Yangtze River basin (YRB) of China during June and July (JJ), which often leads to floods; consequently, it severely affects the ecological environment, agriculture, economy, and human lives (Zong and Chen, 2000; Ding et al., 2021). To mitigate these devastating influences, it is important to explore factors that precede the EASM precipitation, especially for the JJ YRB precipitation.

✱ This paper is a contribution to the 2nd Special Issue on Climate Science for Service Partnership China.

\* Corresponding author: Ge LIU  
Email: [liuge@cma.gov.cn](mailto:liuge@cma.gov.cn)

El Niño–Southern Oscillation (ENSO) has been widely considered one of the most important factors affecting the variation of the EASM on different time scales (Zhang et al., 1999; Wu and Wang, 2002; Chen et al., 2013). ENSO can contribute to the YRB precipitation anomaly in summer by modulating the East Asia-Pacific (EAP) pattern (Huang et al., 2004; Feng et al., 2011). The positive (negative) EAP pattern is characterized by an anomalous anticyclone (cyclone) over the tropical western North Pacific (WNP) and an anomalous cyclone (anticyclone) at the middle latitudes of East Asia in the lower troposphere, which is also accompanied by a southward (northward) shift of the East Asian westerly jet (EAJ) at the upper troposphere (Li et al., 2021b). The ENSO-related positive (negative) EAP pattern is conducive to more (less) precipitation over the YRB and southern Japan (Lu, 2004; Li et al., 2021b). Additionally, the sea surface temperature (SST) anomalies in the North Pacific, the North Atlantic Ocean (Guo et al., 2017), and the tropical Indian Ocean (Xie et al., 2009; Ding et al., 2021) can affect the EASM precipitation.

Apart from the above SST factors, land conditions have also received much attention. For example, Xue et al. (2018) reported that spring land surface or subsurface temperature anomalies in the Tibetan Plateau (TP) could improve the prediction of dry and wet conditions, especially extreme drought/flood events around the YRB. Through altering local hydrological and thermal processes and the associated overlying and downstream atmospheric circulations, the snow cover and soil moisture anomalies in the TP during winter or spring can affect summer precipitation over the YRB (Wu and Qian, 2003; Wu and Kirtman, 2007; Zhao et al., 2007a; Chow et al., 2008; Liu et al., 2014; Wang et al., 2017). However, the close relationship between the preceding TP snow and summer YRB precipitation has been disrupted since the late 1990s due to the decreasing winter TP snow associated with the TP warming (Si and Ding, 2013; Xu et al., 2017). Moreover, the complex land surface environment in the TP severely affected the quality of the snow and heat flux datasets (Chen et al., 2021), leading to inconsistent variations of variables in the TP among different datasets (Bian et al., 2020). As such, alternative variables should be explored to predict the YRB precipitation aside from traditional land surface variables (e.g., snow and surface heat fluxes) in the TP.

Recently, several studies revealed that the TP tropospheric temperature (TPTT) could reflect the thermal condition of the TP and has better regional coherence than land surface variables (Nan et al., 2019, 2021). Moreover, Chen et al. (2021) found that the preceding spring TPTT considerably impacts summer precipitation over eastern China, especially over the North China–Hetao region. Inspired by previous studies, the present study explores the potential signal for summer precipitation over the YRB from the TPTT during the preceding months.

The remainder of this paper is organized as follows. Section 2 describes the data and methods. Section 3 analyzes the relationship between the JJ YRB precipitation and the pre-

ceding winter TPTT. The link between the TPTT and the tropical SSTs and the respective contribution of the TPTT and SST anomalies to the YRB precipitation are also investigated in section 3. Section 4 explores the potential memory process of winter TPTT anomaly that leads to the summer anomaly, which explains how the winter TPTT anomaly can affect the summer atmospheric circulation pattern and associated precipitation over the YRB. Finally, the summary and discussion are given in section 5.

## 2. Data and methods

### 2.1. Data

This study used the monthly precipitation data at 160 observational stations in China, which were obtained from the National Meteorological Information Center, China Meteorological Administration. The precipitation product of the Climate Prediction Center (CPC) Merged Analysis of Prediction (CMAP; Xie and Arkin, 1997) was used to verify the results. This study also used the monthly reanalysis data, such as air temperatures, geopotential heights, and winds, obtained from the National Centers for Environmental Prediction and National Center for Atmospheric Research (NCEP–NCAR) (Kalnay et al., 1996). The NCEP–NCAR reanalysis products are updated more rapidly and frequently, which enables the timely calculation of the preceding TPTT, and can therefore be applied in the prediction of the summer precipitation over the YRB.

In addition, we employed the National Oceanic and Atmospheric Administration (NOAA) extended reconstructed SSTs (version 5; Huang et al., 2017) and monthly mean soil temperature at layers 1 (0–7 cm) and 4 (100–289 cm) from the ERA5 reanalysis (Hersbach et al., 2020). All of these data were extracted from 1981–2020 unless otherwise stated.

### 2.2. Methods

We used a rotated empirical orthogonal function (REOF; Richman, 1986) to extract the dominant pattern of precipitation over eastern China since the REOF has a good performance in capturing regional coherence features (Kim and Wu, 1999). In addition, correlation and regression were used in this study. To reveal the relationship between the preceding TPTT and JJ precipitation over the YRB on interannual time scales, we applied eight-year high pass Lanczos filtering (Duchon, 1979) to extract the interannual components from the raw variables. To clarify the independent effect of the TPTT after removing the impact of the SST anomalies, we used the methods of partial correlation (Velleman and Welsch, 1981) and partial regression (Baba et al., 2004). Unless otherwise stated, the Student's *t*-test was used to evaluate the statistical significance of these analyses.

### 2.3. Study domain

The main rain belt generally governs the YRB during JJ and contributes to most EASM precipitation (Chen and

Chang, 1980; Wang et al., 2008). We performed a REOF analysis for the standardized precipitation over eastern China in JJ. Based on the Scree test (Cattel, 1966), the first 10 EOF modes are chosen to be rotated. Their cumulative percent variance is only 60% which indicates that the percent variance of every mode was not as high as expected. The leading REOF mode, which accounts for 7.5% of the total variance of JJ precipitation over eastern China, shows high loadings over the YRB (Fig. 1a). This result further confirms that the main EASM rain belt appears over the YRB during JJ. To measure the variability of precipitation over the YRB, the arithmetical mean of precipitation at 16 observational stations in the YRB ( $27^{\circ}$ – $31^{\circ}$  N,  $107^{\circ}$ – $120^{\circ}$  E) was referred to as the YRB precipitation index (YRBPI). This study focuses on the effect of the preceding TPTT signal on the variability of JJ YRB precipitation.

### 3. Relationship between the JJ YRB precipitation and preceding winter TPTT

#### 3.1. Cross-seasonal relationship between TPTT and YRB precipitation

We explored the preceding signals of the JJ YRB precipitation from the tropospheric eddy temperature ( $T'$ ), in which  $T'$  was defined as the deviation of air temperature ( $T$ ) from the zonal mean (Zhao et al., 2007b). The elevated heating over the TP can be effectively distinguished from the thermal condition at the same latitudes by using  $T'$ . Therefore,  $T'$  can be applied to measure the variability of the TP thermal condition. The JJ YRBPI significantly correlates with December–January (DJ) tropospheric  $T'$  over the TP, with a center of correlation coefficient lower than  $-0.50$  (Fig. 1b). Based on the key area with significant correlation in Fig. 1b, the tropospheric (500–250 hPa)  $T'$  was regionally averaged over ( $25^{\circ}$ – $40^{\circ}$  N,  $80^{\circ}$ – $100^{\circ}$  E) to reflect the variability of the TPTT. For ease of understanding, the TPTT index (TPTTI) was defined as the above regional mean  $T'$  multiplied by  $-1$ . As such, a higher (lower) TPTTI, which reflects lower (higher) tropospheric  $T'$  over the TP during DJ, corresponds to more (less) YRB precipitation in JJ. This relationship can also be detected in Fig. 1c, which shows a clear in-phase fluctuation between the DJ TPTTI and JJ YRBPI, with a correlation coefficient of 0.57, which exceeds the 99.9% confidence level.

Furthermore, we investigated the relationship between the DJ TPTTI and JJ YRBPI on interannual time scales. After extracting the interannual components using high pass Lanczos filtering (Duchon, 1979), the correlation coefficient between DJ TPTTI and JJ YRBPI is 0.53, still significant at the 95% confidence level. The significant correlation suggests that the close relationship between the DJ TPTTI and JJ YRBPI still exists on interannual time scales.

#### 3.2. Associated atmospheric circulation anomalies

Before clarifying the role of the preceding DJ TPTT, we first present the atmospheric circulation anomalies

responsible for anomalous precipitation over the YRB during JJ. The 700 hPa wind anomalies regressed upon the YRBPI show an anomalous anticyclone over the tropical WNP (Fig. 2a), reflecting the strengthened and westward

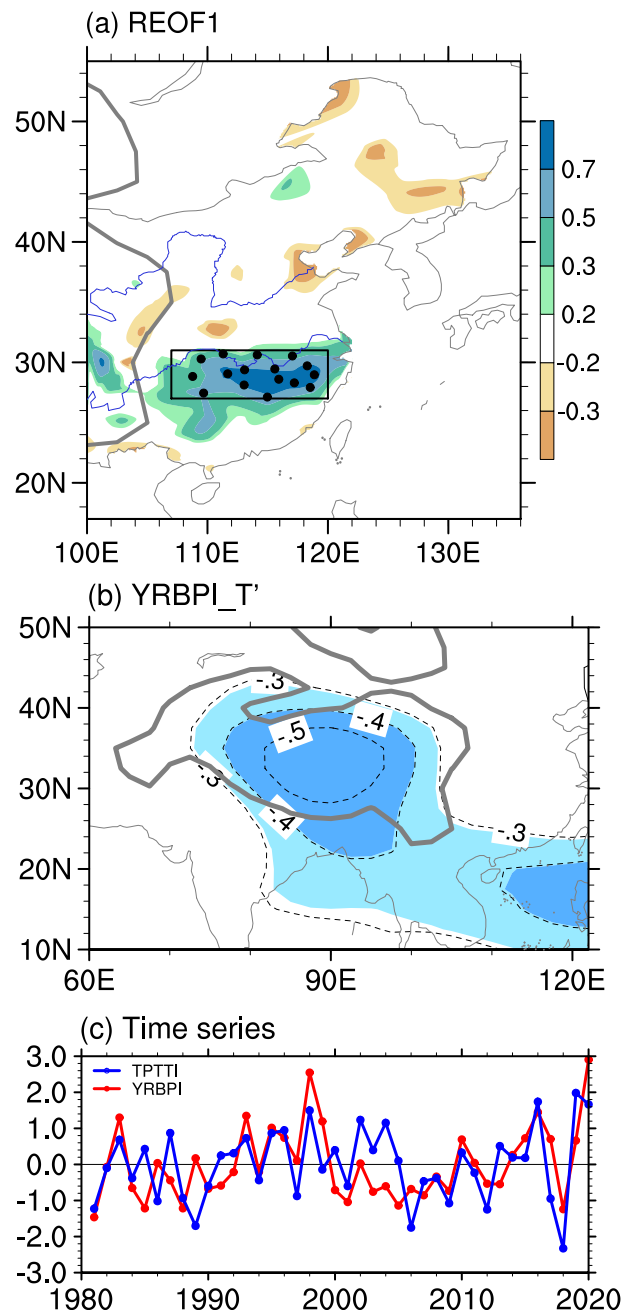


**Fig. 1.** (a) Leading REOF mode of standardized JJ precipitation over eastern China from 1981–2020. The black box represents the YRB region ( $27^{\circ}$ – $31^{\circ}$  N,  $107^{\circ}$ – $120^{\circ}$  E), in which 16 stations are marked by black dots. (b) Correlation between the JJ YRBPI and 500–250 hPa  $T'$  during the preceding DJ, where light and dark blue shadings denote correlations significant at the 95% and 99% confidence levels, respectively. (c) Time series of the standardized JJ YRBPI (red curves) and the preceding DJ TPTTI (blue curves). The bold gray contours in (a) and (b) show the topographic boundary of 1500 m.



extended WNP subtropical high (WNPSH). To the north of the anomalous anticyclone, an anomalous cyclone appears from the east of the TP to the west of southern Japan (Fig. 2a). Along its western flank, the anomalous cyclone induces anomalous northeasterlies into the YRB. The anomalous northeasterlies converge with the anomalous westerlies along the northern flank of the WNPSH, resulting in more precipitation over the YRB. Correspondingly, the 200 hPa zonal wind anomalies show a large-scale positive anomaly belt over East Asia and the WNP, to the south of the climatological EAJ (Fig. 2b), indicating a southward shift of the EAJ. The pattern of the anomalous anticyclone over the tropical WNP and the anomalous cyclone at middle latitudes and the southward shifted EAJ reflect the positive phase of the EAP pattern, which is conducive to excessive precipitation over the YRB compared to the individual contributions of either the WNPSH or EAJ (Li et al., 2021b).

Clearly, the JJ atmospheric circulation anomalies regressed upon the DJ TPTTI (Figs. 2c, d) also manifest the EAP pattern, which resembles the circulation anomalies responsible for more precipitation over the YRB (Figs. 2a, b). This resemblance implies that the preceding DJ TPTT may influence the YRB precipitation by modulating the EAP teleconnection during JJ. Note that in Fig. 2d, significant

positive anomalies in the 200 hPa zonal winds are confined to eastern China, rather than farther east, over the sea (Fig. 2b). Accordingly, the significant precipitation anomaly appears only over the YRB (Fig. 2c), rather than extending eastward to southern Japan (Fig. 2a).

### 3.3. Respective contribution of DJ TPTT and ENSO

Previous studies pointed out that ENSO can affect winter surface air temperature and snow depth through modulating convective activities over the western Pacific and stimulating the eastward propagation of Rossby waves (Shaman and Tziperman, 2005; Jiang et al., 2019), which implies that the TPTT anomaly is probably also related to ENSO. If so, the close relationship between the DJ TPTT and JJ YRB precipitation may be solely a result of the modulation by ENSO rather than real causality. Therefore, we should further analyze the relationship between the TPTT and ENSO and elucidate the individual contribution of the preceding TPTT to YRB precipitation in the absence of the ENSO.

Figure 3a illustrates the correlation between the DJ TPTTI and simultaneous SSTs, which shows significant positive (negative) correlation coefficients in the equatorial central and eastern Pacific (the tropical WNP), clearly manifesting the positive phase of ENSO. The lead-lag correlation

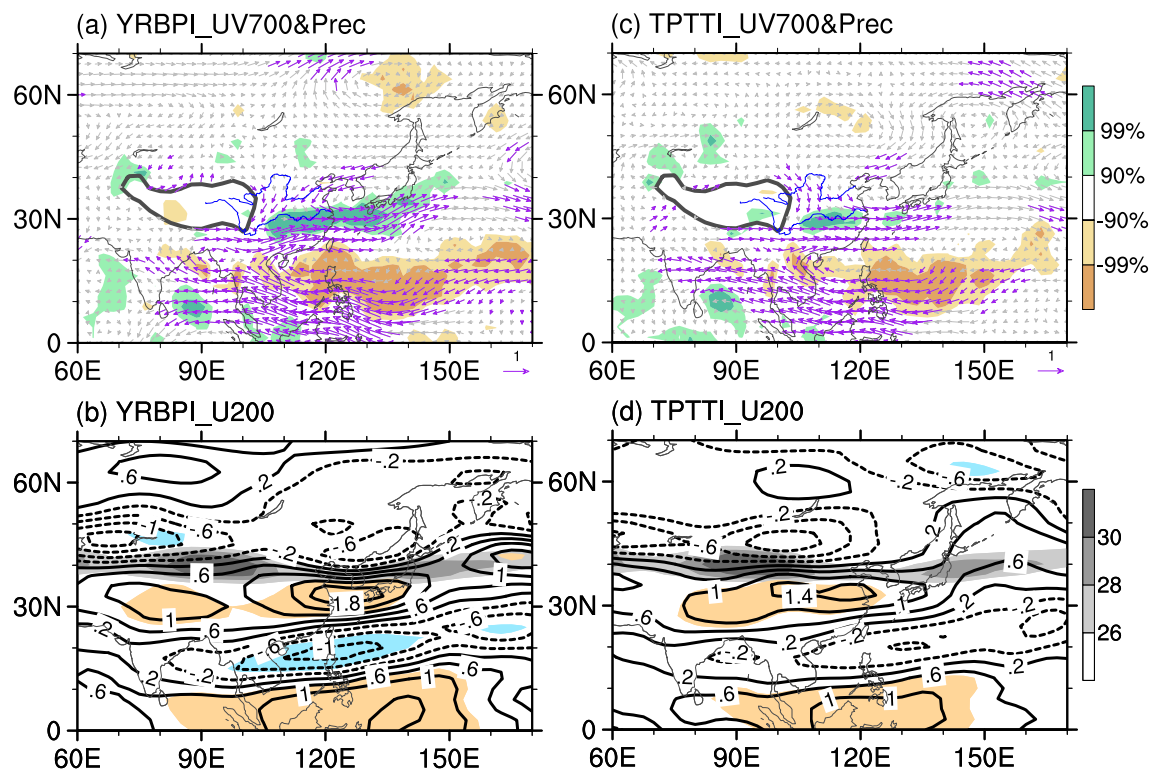


**Fig. 2.** (a) JJ anomalous 700 hPa winds (vectors, units:  $\text{m s}^{-1}$ ) and precipitation (shadings) regressed upon the simultaneous YRBPI. The shadings denote the precipitation anomalies significant at 90% and 99% confidence levels, as shown by the color bars. The anomalous winds significant at the 95% confidence level are highlighted in purple. (b) As in (a), but for the anomalous 200 hPa zonal winds (contours, units:  $\text{m s}^{-1}$ ). In (b), the color shadings denote the anomalous 200 hPa zonal winds significant at the 95% confidence level. The gray shading represents the climatological East Asian westerly jet with westerly winds greater than  $26 \text{ m s}^{-1}$ . Panels (c) and (d), as in (a) and (b), but for the regression upon the preceding DJ TPTTI. The bold gray curves in (a) and (c) delineate the topographic boundary of 3000 m.

between the DJ TPTTI and equatorial ( $5^{\circ}\text{S}$ – $5^{\circ}\text{N}$ ) SST further reveals that the positive correlation in the equatorial Pacific can be traced to spring (April–May) of the preceding year. This positive correlation is enhanced and extends eastward

to the eastern Pacific in the simultaneous winter and decays in the ensuing spring (figure not shown). This result signifies that the variability of TPTT is closely linked to the evolution of ENSO and that this link is more significant at the peak of the ENSO event during DJ.

Similarly, the JJ YRBPI is significantly and positively correlated with the preceding DJ SSTs in the tropical central and eastern Pacific, with the correlation coefficients above 0.40 to the east of  $140^{\circ}\text{W}$ , significant at the 99% confidence level (Fig. 3b). Clearly, the DJ SST in the eastern Pacific (EP;  $5^{\circ}\text{S}$ – $5^{\circ}\text{N}$ ,  $80^{\circ}$ – $140^{\circ}\text{W}$ ) is closely related to both the DJ TPTT and JJ YRB precipitation. Based on Fig. 3, the area-mean SSTs over the EP were defined as the EPSSTI, which can reflect the variability of the ENSO. The correlation coefficient between the DJ EPSSTI and DJ TPTTI (JJ YRBPI) is 0.54 (0.45), significant at the 99.9% (99%) confidence level. The significant correlations imply that the ENSO may play a role in the close relationship between the TPTT and YRB precipitation.

Nevertheless, further analysis reveals that the effect of the preceding DJ TPTT on the JJ YRB precipitation may still exist in the absence of ENSO. After removing the variability of the DJ EPSSTI, the partial regression upon the individual DJ TPTTI shows that the anomalous anticyclone over the WNP still exists (Fig. 4a), although much weaker than that in Fig. 2c. In contrast, the anomalous anticyclone over Northeast Asia and the anomalous cyclone from the east of the TP to the west of southern Japan are strong

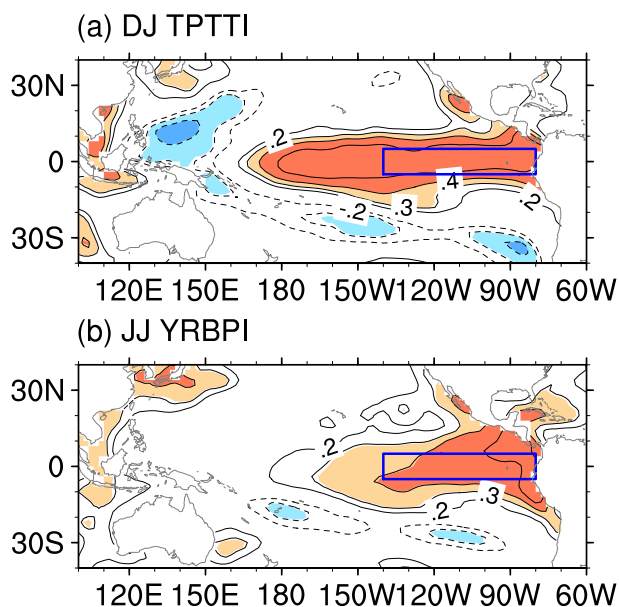


**Fig. 3.** Correlation of the DJ SSTs with the (a) DJ TPTTI and (b) JJ YRBPI. The light and dark shadings denote correlations significant at 95% and 99% confidence levels, respectively. The blue boxes denote the EP region ( $5^{\circ}\text{S}$ – $5^{\circ}\text{N}$ ,  $80^{\circ}$ – $140^{\circ}\text{W}$ ) that was used to define the EPSSTI.

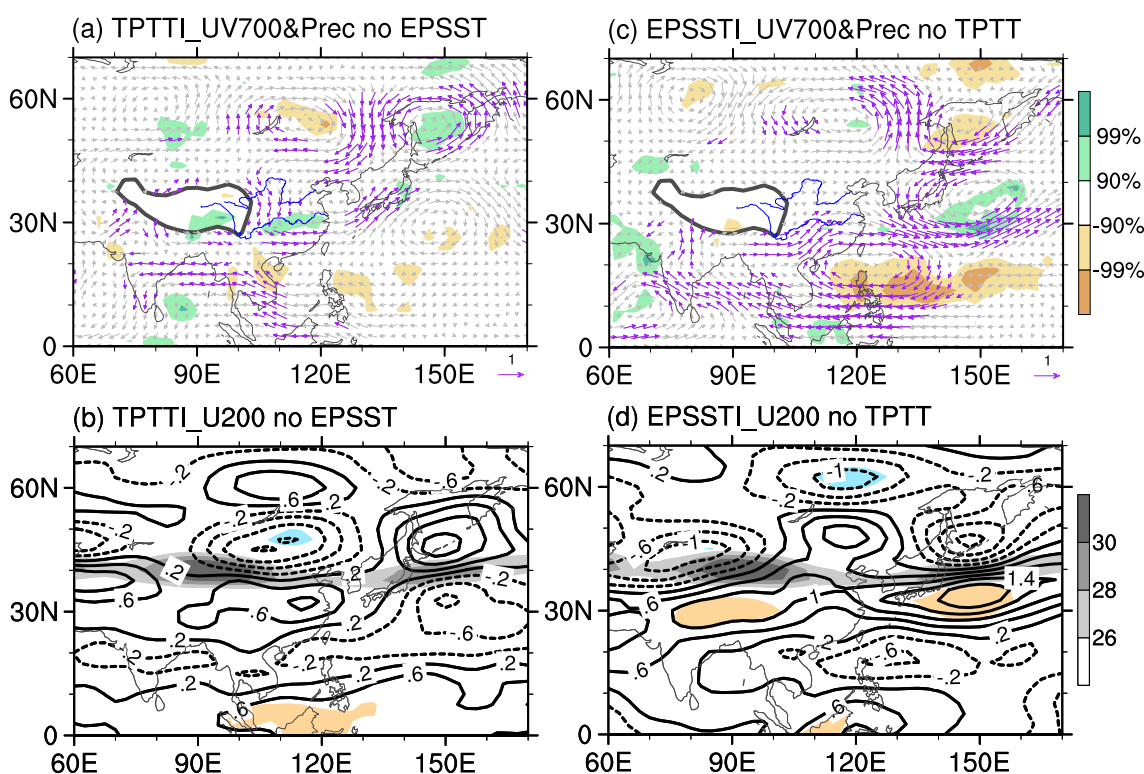


**Fig. 4.** As in Fig. 2, but for the partial regression upon the individual DJ TPTTI after removing the variability of the DJ EPSSTI (a, b). Panels (c) and (d) are similar to (a) and (b), but for the partial regression upon the individual DJ EPSSTI after removing the variability of the DJ TPTTI.

(Fig. 4a). These results suggest that the DJ TPTT exerts a more important influence on atmospheric circulation in the middle and high latitudes during the following JJ. Along the western flank of the anomalous cyclone, the anomalous northeasterlies appear and converge with the anomalous westerlies along the northern flank of the WNPSH, causing more precipitation over the YRB (shadings in Fig. 4a). At 200 hPa, the westerly anomalies to the south of the climatological EAJ are confined to eastern China (Fig. 4b), similar to Fig. 2d, despite the decrease in the significance of zonal wind anomalies. The westerly anomalies are conducive to more precipitation over the YRB to some extent. Consequently, after excluding the effect of the ENSO, the DJ TPTTI still significantly correlates with the JJ YRBPI, with a correlation coefficient of 0.43 (significant at the 99% confidence level).

After removing the variability of DJ TPTT, the regression upon the individual DJ EPSSTI shows a strong anomalous anticyclone over the tropical WNP (Fig. 4c), which indicates that the preceding ENSO can affect the JJ WNPSH through air-sea interactions (Wang et al., 2003). Different from Fig. 4a, an anomalous cyclone appears to the southeast of Japan (Fig. 4c), which guides the anomalous northerlies to the Pacific rather than the YRB. Meanwhile, the 200 hPa westerly anomaly extends eastward, with a center of significant anomalies to the southeast of Japan. As a result, the individual DJ EPSSTI is significantly correlated with the JJ precipitation over the WNP rather than the YRB (shadings in Fig. 4c). The correlation coefficient between the preceding DJ individual EPSSTI and JJ YRBPI is only 0.21 (insignificant).

The above-mentioned results suggest that the preceding DJ TPTT primarily modulates mid-to-high latitude atmospheric circulations, including the anomalous anticyclone around Lake Baikal and the anomalous cyclone extending from the east of the TP to the west of southern Japan during JJ. At the same time, the DJ EP SST generally leads to an anomalous WNPSH. This difference implies that the contribution of the TPTT signal is distinct from and complementary to that of the tropical Pacific signal. Moreover, the independent effect of the preceding TPTT seems sufficient to modulate the precipitation over the YRB during JJ. Next, we further explore why the preceding DJ TPTT can cross-seasonally modulate atmospheric circulation and relevant precipitation over the YRB during JJ.

## 4. Possible mechanisms

### 4.1. Reasons for the persistence of the TPTT anomaly

The cross-seasonal relationship between the preceding DJ TPTT and JJ YRB precipitation may be attributed to the persistence of the TPTT from DJ to JJ. Figure 5a depicts the lead-lag correlation between the DJ TPTTI and area-mean  $T'$  over the TP region ( $25^{\circ}$ – $40^{\circ}$ N,  $80^{\circ}$ – $100^{\circ}$ E) at different levels from November–December (ND) of the previous year to October–November (ON) in the current year. In this figure, we can detect that the upper-tropospheric (300–150 hPa)  $T'$

anomaly over the TP region can persist from DJ to JJ (Fig. 5a). This persistence greatly weakens after removing the contribution of preceding DJ EP SST (Fig. 5b), illustrating the importance of the ENSO in maintaining the TPTT anomaly above 500 hPa. Moreover, the correlation analyses further show that the DJ EPSSTI is significantly correlated with the 300–200 hPa temperatures over the TP during JJ, but not with the 600–500 hPa temperatures (figure omitted). This result further confirms the importance of the ENSO in keeping the TPTT signal above 500 hPa.

The individual TPTT in DJ is still significantly correlated with the tropospheric  $T'$  below 500 hPa in JJ, even though this relationship breaks in spring (Fig. 5b). This close connection in lower levels implies that the land-air interaction may serve as a signal persisting role. Recently, several studies have reported the effect of land surface and subsurface temperature on downstream droughts/floods (Xue et al., 2018; Diallo et al., 2019). The memory of subsurface temperature in the TP persists for up to 1–3 months and even longer in deeper soil (Liu et al., 2020). Through the long memory, the subsurface soil probably preserves the surface thermal signal and affects the overlaying tropospheric temperature in the following months.

To examine whether the subsurface soil can play an important role in linking the DJ TPTT with the tropospheric  $T'$  below 500 hPa over the TP in JJ, we examined the correlation between the DJ TPTTI and subsurface soil temperatures in the TP during the ensuing spring, i.e., March, April, and May (MAM) (Fig. 6). The correlation analyses show that the DJ TPTT has a closer relationship with deep-layer

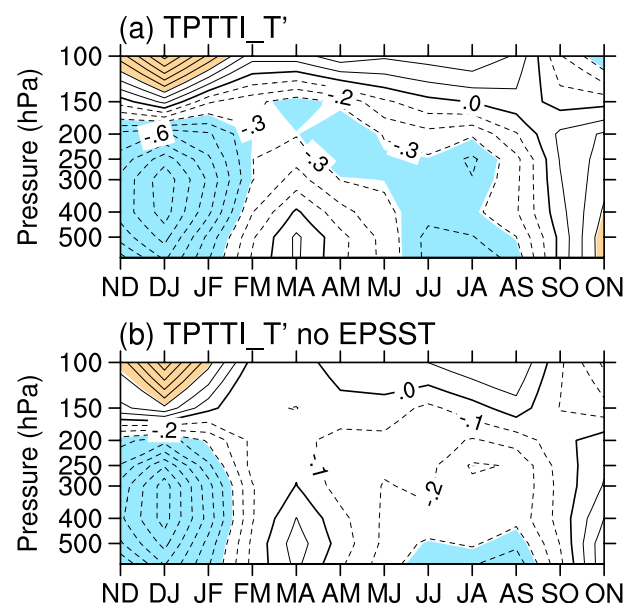


**Fig. 5.** (a) Lead-lag correlation between the DJ TPTTI and area-mean  $T'$  over the TP region ( $25^{\circ}$ – $40^{\circ}$ N,  $80^{\circ}$ – $100^{\circ}$ E) at different levels from November–December (ND) of the previous year to October–November (ON) in the current year. (b) As in (a), but for the partial correlation after removing the variability of the DJ EPSSTI. Shadings denote correlations significant at the 95% confidence level.



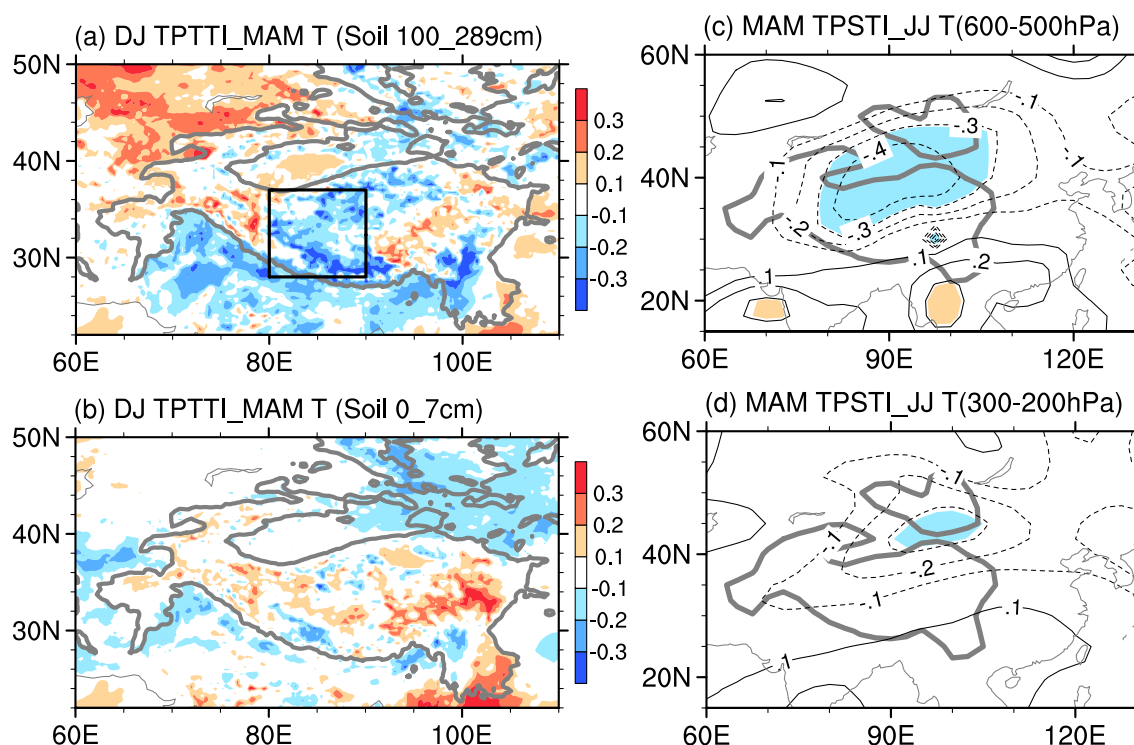


**Fig. 6.** Correlation between the preceding DJ TPTTI and spring (MAM) soil temperatures in (a) deep (100–289 cm) and (b) shallow (0–7 cm) layers. Correlation between the MAM TPSTI and JJ tropospheric temperatures at (c) 600–500 and (d) 300–200 hPa levels. Shadings in (c) and (d) denote correlations significant at the 95% confidence level. The black box in (a) denotes the central TP region (28°–37°N, 80°–90°E) that was used to define the TPSTI. Bold gray lines delineate the topographic boundary of 1500 m.

(100–289 cm) soil temperatures in the TP (Fig. 6a), rather than with shallow-layer (0–7 cm) soil temperatures (Fig. 6b). According to the key area (see the box in Fig. 6a) of high correlation, the TP soil temperature index (TPSTI) was defined as the area-mean deep-layer soil temperature over the central TP (28°–37°N, 80°–90°E), which was also multiplied by  $-1$ , in agreement with the definition of the TPTTI.

The interannual correlation between the spring TPSTI and JJ 600–500 hPa air temperature shows a significant negative correlation over the central TP extending northeastward (Fig. 6c). However, the correlation between the spring TPSTI and JJ air temperature above 500 hPa is much weaker (Fig. 6d). The above results suggest that the deep-layer soil temperature modulates the TPTT below 500 hPa, but has a weaker effect on the TPTT above 500 hPa during JJ. The persistence of the anomalous TPTT signal below 500 hPa is broken during spring (Fig. 5b), possibly due to a lack of significant anomalies preserved in the spring shallow-layer soil temperature that can directly affect the TPTT below 500 hPa. Instead, the anomalous TPTT signal may be preserved in deep-layer soil temperatures during spring and released to affect the TPTT below 500 hPa during JJ. As such, a TPTT anomaly, which is consistent with the DJ TPTT, appears below 500 hPa from JJ to August–September (AS) (Fig. 5b). Notably, this is only a preliminary speculation. The specific process of heat transport between the surface and subsurface requires further investigation in the

future.

The above analyses suggest that the DJ ENSO and MAM TPST modulate the JJ TPTT above and below 500 hPa, respectively. Therefore, the maintenance of the TPTT signal from winter to summer may be attributed to the joint effect of ENSO and the TPST. To reveal this joint effect, the TPST-ENSO index was defined as the sum of the DJ EPSSTI and MAM TPSTI. The TPST-ENSO index is closely correlated with the JJ TPTT above and below 500 hPa (Fig. 7), confirming that the DJ ENSO and MAM TPST may synergistically contribute to the thick TPTT anomaly during JJ. As a result, the DJ TPTT, which relates to both the ocean (ENSO) and land (deep-layer soil temperature) signals, is significantly correlated with the lower and upper tropospheric TPTT (Figs. 8a, b), forming a thick TPTT anomaly during JJ (Fig. 5a). Given the break of persistence of the TPTT anomaly during spring (Fig. 5a), the TPTT signal may not directly persist from winter to summer. However, the preceding DJ TPTT can reflect the JJ TPTT well through the relay modulation of the ENSO and TPST. Therefore, the DJ TPTT can be considered the precursory signal of the variability of the JJ YRB precipitation.

#### 4.2. Mechanisms of the impact of the TPTT on YRB precipitation

Corresponding to a higher TPTTI (i.e., lower TPTT) during the preceding DJ, significantly negative  $T'$  anomalies appear below 500 hPa over the TP during JJ (Fig. 8a) and



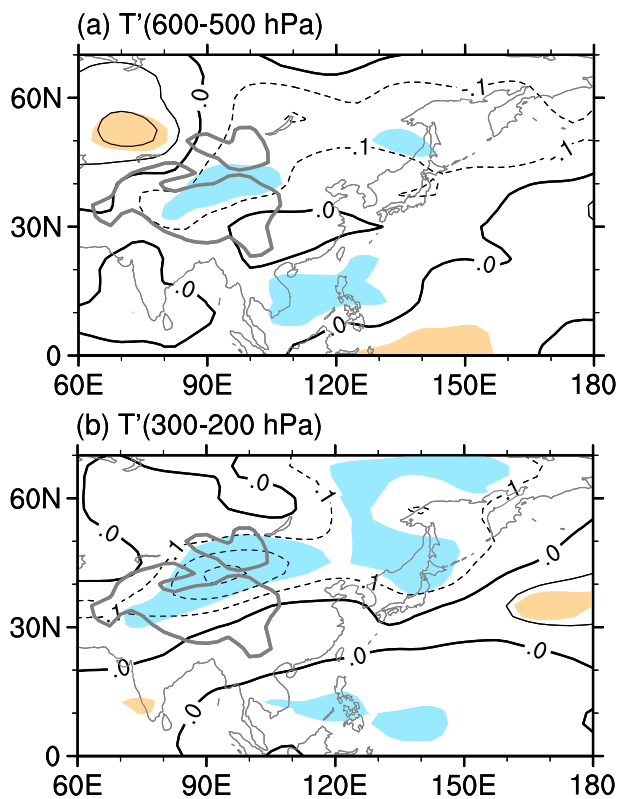


**Fig. 7.** JJ (a) 600–500 and (b) 300–200 hPa  $T'$  anomalies (units:  $^{\circ}\text{C}$ ) regressed upon the preceding TPST-ENSO index. The shadings denote the anomalies significant at the 95% confidence level. The bold gray contour delineates the topographic boundary of 1500 m.

extend northeastward at upper levels (300–200 hPa) from the TP to the east of Lake Baikal (Fig. 8b), constituting a consistent cold air column tilting and extending northeastward from the TP surface to the upper troposphere (Fig. 9a). This configuration is probably related to the variability of the JJ  $T'$  above and below 500 hPa (figures not shown). The belt of significantly lower temperature anomalies at 300–200 hPa enhances the meridional thermal gradient to the south of the belt (Fig. 8c). According to the principle of thermal wind, the enhanced meridional thermal gradient results in anomalous upper-tropospheric westerlies there, reflecting the southward shift of the EAJ (Fig. 2d). This is conducive to more precipitation over the YRB during JJ.

Moreover, the negative  $T'$  anomalies extending from the TP to the east of Lake Baikal (Fig. 8b) can lead to a higher atmospheric density. Under the higher density atmosphere, a high-pressure anomaly and its associated anticyclone tend to be stronger to the east of Lake Baikal, which induces anomalous northeasterlies (Fig. 4a). Meanwhile, an anomalous land-sea thermal contrast appears between the TP and the WNP (Fig. 9a). According to the principle of thermal wind, the enhanced zonal thermal gradient results in anomalous southwesterlies around  $135^{\circ}\text{E}$  in the lower troposphere (Fig. 4a). The anomalous southwesterlies induce a convergence anomaly in the lower troposphere around Japan (figure omitted). Accompanying the lower tropospheric conver-

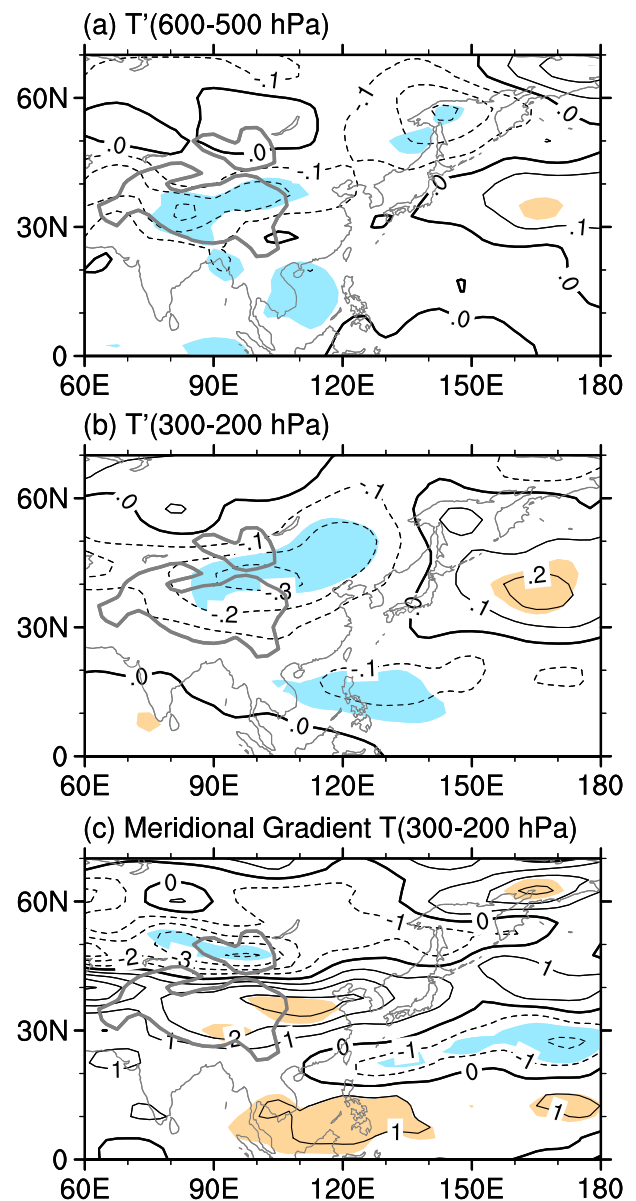


**Fig. 8.** JJ (a) 600–500 and (b) 300–200 hPa  $T'$  anomalies (units:  $^{\circ}\text{C}$ ) regressed upon the preceding DJ TPTI. (c) As in (b), but for the meridional thermal gradient anomalies (units:  $10^{-7}^{\circ}\text{C m}^{-1}$ ). The shadings denote the anomalies significant at the 95% confidence level. The bold gray contour delineates the topographic boundary of 1500 m.

gence, anomalous ascending motion and a related enhancement of convection appear around Japan (figure omitted), which may release more latent heat and further enhance the warming over the WNP along  $35^{\circ}\text{N}$  (Fig. 9a). The subsequent warming over the WNP and cooling over the TP can reinforce the land-sea thermal contrast, which further leads to the anomalous southwesterlies, demonstrating the process of positive feedback. The anomalous northeasterlies to the east of the TP and anomalous southeasterlies around  $135^{\circ}\text{E}$  are conducive to reinforcing the anomalous cyclone from the east of the TP to the west of southern Japan (vectors in Fig. 4a), therefore, facilitating more precipitation over the YRB (shad-

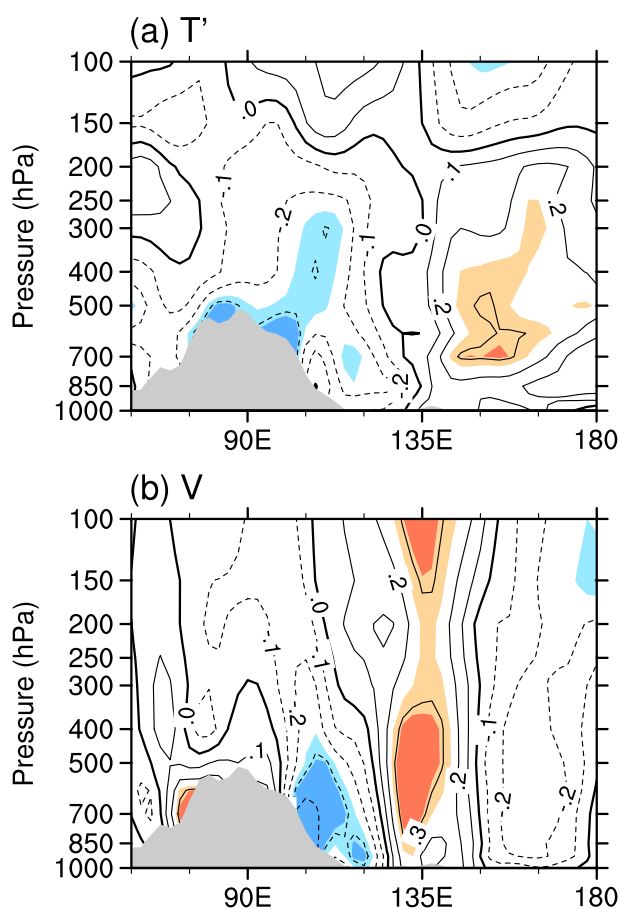


**Fig. 9.** (a) Partial correlation between the preceding DJ individual TPTTI and JJ  $T'$  on a zonal-vertical cross-section along  $35^\circ\text{N}$ , in which the individual TPTTI has removed the variability of DJ EPSSTI. (b) As in (a), but for the partial correlation between the individual TPTTI and meridional winds. The gray shadings denote the topography of the TP. Color shadings denote correlations significant at 90% and 95% confidence levels.

ings in Fig. 4a).

In summary, the JJ TPTT anomaly, which can be reflected by the preceding DJ TPTT anomaly, can modulate precipitation over the YRB by affecting the westerly wind system, the land-sea thermal contrast, and the anomalous cyclone at middle latitudes during JJ.

## 5. Summary and discussion

The prediction of EASM precipitation has long been challenging, especially precipitation over the YRB during JJ when the mei-yu generally occurs. Exploring the precursory signals of JJ YRB precipitation can help alleviate the disastrous impact of droughts/floods. The present study shows that the preceding DJ TPTT is significantly correlated with the JJ YRB precipitation.

Theoretically, the TPTT should be considered a rapidly varying atmospheric signal. Nevertheless, the DJ TPTT has a close connection with the JJ TPTT, although the persistence

of the TPTT signal is weak during spring. Further analyses reveal that the anomalous TPTT signal may be reserved in deep-layer soil temperatures during spring and released to affect the TPTT below 500 hPa during JJ. Meanwhile, the DJ ENSO plays an important role in linking the DJ and following JJ TPTT above 500 hPa. That is, the DJ ENSO and spring TPST may synergistically contribute to the thick TPTT anomaly above and below 500 hPa during JJ. Due to the joint modulation of the ocean (ENSO) and land (TPST) thermal conditions, the DJ TPTT can reflect the JJ TPTT well and consequently affect atmospheric circulation and associated precipitation anomalies over the YRB during JJ.

The effect of the TPTT on atmospheric circulation and relevant YRB precipitation can be simply explained by the following physical processes (Fig. 10). Corresponding to a higher TPTTI (i.e., lower TPTT) during the preceding DJ, the TPTT is still lower during the following JJ. The negative TPTT anomalies extend from the TP to the east of Lake Baikal, resulting in a higher atmospheric density and hence an anomalous high pressure and associated anomalous anticyclone to the east of Lake Baikal. Meanwhile, the intensified land-sea thermal contrast between the TP and the WNP enhances anomalous southwesterlies to the west of southern Japan. As such, the anomalous cyclone is reinforced in the middle latitudes of East Asia. Moreover, an anomalous anticyclone appears over the tropical WNP. Additionally, the lower temperature belt extending from the TP to the east of Lake Baikal enhances the meridional thermal gradient in the upper troposphere, thereby causing a southward shift of the EAJ. The above circulation anomalies resemble the positive EAP anomaly, facilitating more precipitation over the YRB (Fig. 10).

The roles of the DJ TPTT and ENSO in modulating summer atmospheric circulation anomalies are distinctly different. Specifically, the TPTT primarily governs atmospheric circulation at the middle and high latitudes during JJ, while the ENSO generally affects the WNPSH at the lower latitudes. Furthermore, the DJ ENSO contributes to the consistency between the preceding DJ and JJ TPTT signals, to some extent. Clearly, ENSO can directly affect the JJ YRB precipitation by modulating the WNPSH. Besides, ENSO can indirectly affect the JJ YRB precipitation through the “bridge” effect. The TPTT seems to act as a bridge between the ENSO and the JJ YRB precipitation, but it has its own independent effect as it contains both land and ocean signals. The DJ TPTT has a closer relationship with the JJ precipitation over the YRB than the DJ ENSO. The correlation coefficient of the JJ YRBPI with the DJ TPTTI is 0.57, higher than that with the DJ EPSSTI (0.45). As such, the DJ TPTT can be considered the precursory signal of the variability of the JJ YRB precipitation, although its “persistence” is only a result of the relay modulation of the ocean and land signals.

Several important issues deserve further study. For instance, what is the reason that the DJ TPTT signal is transmitted to deep-layer soil during spring and is released into

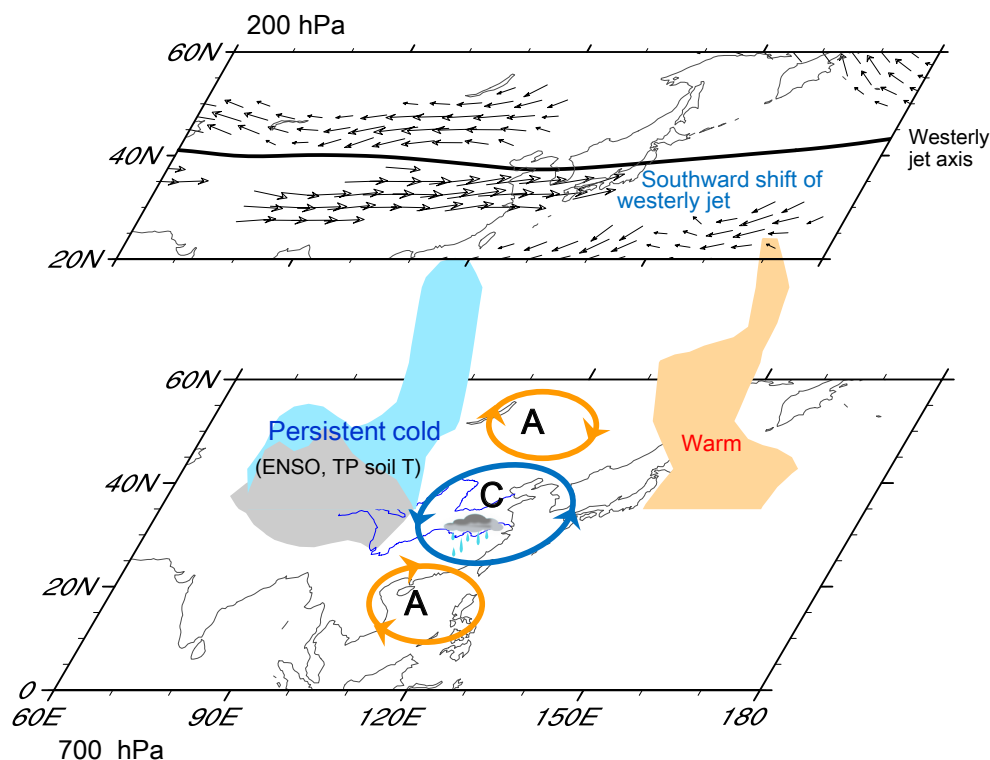


**Fig. 10.** Schematic diagram describing how the TPTT anomaly affects the JJ YRB precipitation. Orange and blue elliptical circles denote anomalous anticyclones (A) and cyclones (C), respectively. The blue shading represents the colder TPTT tilting northeastward from the TP surface to the upper troposphere. The orange shading represents a warmer atmosphere column. The thick black curve represents the axis of the climatological westerly Jet in the upper troposphere. The anomalous westerly (easterly) to the south (north) of this Jet axis reflects the southward shift of the EAJ. The grey shading denotes the TP.

the surface during summer? What are the details of the contribution of the evolution of ENSO to the consistency between the DJ and JJ TPTT anomalies? Besides the ENSO and the TP soil temperature, many other factors are responsible for an anomalous TPTT. For example, a strong TP monsoon can cause middle and upper tropospheric cooling (Zhao et al., 2019; Zhang et al., 2022). In light of this, is it possible that the TP monsoon can affect summer precipitation over the YRB by adjusting the TPTT? This conjecture deserves further exploration. In addition to the effect of the TPTT, TP vortices, which are related to the EAP pattern, may also affect the precipitation over eastern China (Yu et al., 2015; Li et al., 2021a). The potential connection between the TPTT and TP vortices and the joint contribution to the YRB precipitation warrant further investigation in the future.

**Acknowledgements.** This work was jointly sponsored by the National Key Research and Development Program of China (Grant No. 2018YFC1501706), the Second Tibetan Plateau Scientific Expedition and Research (STEP) program (Grant No. 2019QZKK0105), National Natural Science Foundation of China (Grant No. 41975088), the Strategic Priority Research Program of the Chinese Academy of Sciences (Grant No. XDA20100300), and the Basic Research Fund of CAMS (Grants No. 2021Z007).

## REFERENCES

- Baba, K., R. Shibata, and M. Sibuya, 2004: Partial correlation and conditional correlation as measures of conditional independence. *Australian and New Zealand Journal of Statistics*, **46**(4), 657–664, <https://doi.org/10.1111/j.1467-842X.2004.00360.x>.
- Bian, Q. Y., and Coauthors, 2020: Multiscale changes in snow over the Tibetan Plateau during 1980–2018 represented by reanalysis data sets and satellite observations. *J. Geophys. Res.: Atmos.*, **125**, e2019JD031914, <https://doi.org/10.1029/2019JD031914>.
- Cattell, R. B., 1966: The Scree test for the number of factors. *Multivariate Behavioral Research*, **1**(2), 245–276, [https://doi.org/10.1207/s15327906mbr0102\\_10](https://doi.org/10.1207/s15327906mbr0102_10).
- Chen, D., S. L. Nan, G. Liu, C. Y. Zhou, R. R. Shi, Y. H. Ao, and X. Li, 2021: Improvement in the prediction of summer precipitation in the North China–Hetao region using the tropospheric temperature over the Tibetan Plateau in spring. *Frontiers in Earth Science*, **9**, 708567, <https://doi.org/10.3389/feart.2021.708567>.
- Chen, T. J. G., and C.-P. Chang, 1980: The structure and vorticity budget of an early summer monsoon trough (Mei-Yu) over southeastern China and Japan. *Mon. Wea. Rev.*, **108**, 942–953, [https://doi.org/10.1175/1520-0493\(1980\)108<0942:TSAVBO>2.0.CO;2](https://doi.org/10.1175/1520-0493(1980)108<0942:TSAVBO>2.0.CO;2).
- Chen, W., J. Feng, and R. G. Wu, 2013: Roles of ENSO and

- PDO in the link of the East Asian winter monsoon to the following summer monsoon. *J. Climate*, **26**, 622–635, <https://doi.org/10.1175/JCLI-D-12-00021.1>.
- Chow, K. C., J. C. L. Chan, X. L. Shi, Y. M. Liu, and Y. H. Ding, 2008: Time-lagged effects of spring Tibetan Plateau soil moisture on the monsoon over China in early summer. *International Journal of Climatology*, **28**(1), 55–67, <https://doi.org/10.1002/joc.1511>.
- Diallo, I., Y. K. Xue, Q. Li, F. De Sales, and W. Li, 2019: Dynamical downscaling the impact of spring western US land surface temperature on the 2015 flood extremes at the Southern Great Plains: Effect of domain choice, dynamic cores and land surface parameterization. *Climate Dyn.*, **53**(1–2), 1039–1061, <https://doi.org/10.1007/s00382-019-04630-6>.
- Ding, Y. H., Y. Y. Liu, and Z.-Z. Hu, 2021: The record-breaking Mei-yu in 2020 and associated atmospheric circulation and tropical SST anomalies. *Adv. Atmos. Sci.*, **38**, 1980–1993, <https://doi.org/10.1007/s00376-021-0361-2>.
- Duchon, C. E., 1979: Lanczos filtering in one and two dimensions. *J. Appl. Meteorol. Climatol.*, **18**, 1016–1022, [https://doi.org/10.1175/1520-0450\(1979\)018<1016:LFIOAT>2.0.CO;2](https://doi.org/10.1175/1520-0450(1979)018<1016:LFIOAT>2.0.CO;2).
- Feng, J., W. Chen, C. Y. Tam, and W. Zhou, 2011: Different impacts of El Niño and El Niño Modoki on China rainfall in the decaying phases. *International Journal of Climatology*, **31**, 2091–2101, <https://doi.org/10.1002/joc.2217>.
- Guo, Y., J. P. Li, and J. S. Zhu, 2017: A moving updated statistical prediction model for summer rainfall in the middle-lower reaches of the Yangtze River valley. *J. Appl. Meteorol. Climatol.*, **56**, 2275–2287, <https://doi.org/10.1175/JAMC-D-16-0376.1>.
- Hersbach, H., and Coauthors, 2020: The ERA5 global reanalysis. *Quart. J. Roy. Meteor. Soc.*, **146**, 1999–2049, <https://doi.org/10.1002/qj.3803>.
- Huang, B. Y., and Coauthors, 2017: Extended reconstructed sea surface temperature, version 5 (ERSSTv5): Upgrades, validations, and intercomparisons. *J. Climate*, **30**, 8179–8205, <https://doi.org/10.1175/JCLI-D-16-0836.1>.
- Huang, R. H., W. Chen, B. L. Yang, and R. H. Zhang, 2004: Recent advances in studies of the interaction between the East Asian winter and summer monsoons and ENSO cycle. *Adv. Atmos. Sci.*, **21**, 407–424, <https://doi.org/10.1007/BF02915568>.
- Jiang, X. W., T. T. Zhang, C.-Y. Tam, J. W. Chen, N. C. Lau, S. Yang, and Z. Y. Wang, 2019: Impacts of ENSO and IOD on snow depth over the Tibetan Plateau: Roles of convections over the western North Pacific and Indian Ocean. *J. Geophys. Res.: Atmos.*, **124**, 11 961–11 975, <https://doi.org/10.1029/2019JD031384>.
- Kalnay, E., and Coauthors, 1996: The NCEP/NCAR 40-year reanalysis project. *Bull. Amer. Meteor. Soc.*, **77**, 437–472, [https://doi.org/10.1175/1520-0477\(1996\)077<0437:TNYRP>2.0.CO;2](https://doi.org/10.1175/1520-0477(1996)077<0437:TNYRP>2.0.CO;2).
- Kim, K. Y., and Q. G. Wu, 1999: A comparison study of EOF techniques: Analysis of nonstationary data with periodic statistics. *J. Climate*, **12**, 185–199, <https://doi.org/10.1175/1520-0442-12.1.185>.
- Li, L., C. W. Zhu, R. H. Zhang, and B. Q. Liu, 2021a: Roles of the Tibetan Plateau vortices in the record Meiyu rainfall in 2020. *Atmospheric Science Letters*, **22**, e1017, <https://doi.org/10.1002/asl.1017>.
- Li, X. Y., R. Y. Lu, and G. Li, 2021b: Different configurations of interannual variability of the western North Pacific subtropical high and East Asian westerly jet in summer. *Adv. Atmos. Sci.*, **38**(6), 931–942, <https://doi.org/10.1007/s00376-021-0339-0>.
- Liu, G., R. G. Wu, and Y. Z. Zhang, 2014: Persistence of snow cover anomalies over the Tibetan Plateau and the implications for forecasting summer precipitation over the Meiyu–Baiu region. *Atmos. Ocean. Sci. Lett.*, **7**(2), 115–119, <https://doi.org/10.1080/16742834.2014.11447145>.
- Liu, Y., Y. K. Xue, Q. Li, D. Lettenmaier, and P. Zhao, 2020: Investigation of the variability of near-surface temperature anomaly and its causes over the Tibetan Plateau. *J. Geophys. Res.: Atmos.*, **125**, e2020JD032800, <https://doi.org/10.1029/2020JD032800>.
- Lu, R. Y., 2004: Associations among the components of the East Asian summer monsoon system in the meridional direction. *J. Meteor. Soc. Japan. Ser. II*, **82**, 155–165, <https://doi.org/10.2151/jmsj.82.155>.
- Nan, S. L., P. Zhao, and J. M. Chen, 2019: Variability of summertime Tibetan tropospheric temperature and associated precipitation anomalies over the central-eastern Sahel. *Climate Dyn.*, **52**(3–4), 1819–1835, <https://doi.org/10.1007/s00382-018-4246-8>.
- Nan, S. L., P. Zhao, J. M. Chen, and G. Liu, 2021: Links between the thermal condition of the Tibetan Plateau in summer and atmospheric circulation and climate anomalies over the Eurasian continent. *Atmospheric Research*, **247**, 105212, <https://doi.org/10.1016/j.atmosres.2020.105212>.
- Richman, M. B., 1986: Rotation of principal components. *J. Climatol.*, **6**, 293–335, <https://doi.org/10.1002/joc.3370060305>.
- Shaman, J., and E. Tziperman, 2005: The effect of ENSO on Tibetan Plateau snow depth: A stationary wave teleconnection mechanism and implications for the South Asian monsoons. *J. Climate*, **18**, 2067–2079, <https://doi.org/10.1175/JCLI3391.1>.
- Si, D., and Y. H. Ding, 2013: Decadal change in the correlation pattern between the Tibetan Plateau winter snow and the East Asian summer precipitation during 1979–2011. *J. Climate*, **26**, 7622–7634, <https://doi.org/10.1175/JCLI-D-12-00587.1>.
- Velleman, P. F., and R. E. Welsch, 1981: Efficient computing of regression diagnostics. *The American Statistician*, **35**(4), 234–242, <https://doi.org/10.1080/00031305.1981.10479362>.
- Wang, C. H., K. Yang, Y. L. Li, D. Wu, and Y. Bo, 2017: Impacts of spatiotemporal anomalies of Tibetan Plateau snow cover on summer precipitation in eastern China. *J. Climate*, **30**(3), 885–903, <https://doi.org/10.1175/JCLI-D-16-0041.1>.
- Wang, B., R. G. Wu, and T. Li, 2003: Atmosphere–warm ocean interaction and its impacts on Asian–Australian monsoon variation. *J. Climate*, **16**, 1195–1211, [https://doi.org/10.1175/1520-0442\(2003\)16<1195:AOIAII>2.0.CO;2](https://doi.org/10.1175/1520-0442(2003)16<1195:AOIAII>2.0.CO;2).
- Wang, B., Z. W. Wu, J. P. Li, J. Liu, C. P. Chang, Y. H. Ding, and G. X. Wu, 2008: How to measure the strength of the East Asian summer monsoon. *J. Climate*, **21**, 4449–4463, <https://doi.org/10.1175/2008JCLI2183.1>.
- Wu, R. G., and B. Wang, 2002: A contrast of the East Asian summer monsoon–ENSO relationship between 1962–77 and 1978–93. *J. Climate*, **15**, 3266–3279, [https://doi.org/10.1175/1520-0442\(2002\)015<3266:ACOTEAS>2.0.CO;2](https://doi.org/10.1175/1520-0442(2002)015<3266:ACOTEAS>2.0.CO;2).
- Wu, R. G., and B. P. Kirtman, 2007: Observed relationship of spring and summer East Asian rainfall with winter and spring Eurasian snow. *J. Climate*, **20**(7), 1285–1304, <https://doi.org/10.1175/JCLI3738.06>.



[doi.org/10.1175/JCLI4068.1](https://doi.org/10.1175/JCLI4068.1).

- Wu, T. W., and Z. A. Qian, 2003: The relation between the Tibetan winter snow and the Asian summer monsoon and rainfall: An observational investigation. *J. Climate*, **16**(12), 2038–2051, [https://doi.org/10.1175/1520-0442\(2003\)016<2038:TRBTTW>2.0.CO;2](https://doi.org/10.1175/1520-0442(2003)016<2038:TRBTTW>2.0.CO;2).
- Xie, P. P., and P. A. Arkin, 1997: Global precipitation: A 17-year monthly analysis based on gauge observations, satellite estimates, and numerical model outputs. *Bull. Amer. Meteor. Soc.*, **78**, 2539–2558, [https://doi.org/10.1175/1520-0477\(1997\)078<2539:GPAYMA>2.0.CO;2](https://doi.org/10.1175/1520-0477(1997)078<2539:GPAYMA>2.0.CO;2).
- Xie, S. P., K. M. Hu, J. Hafner, H. Tokinaga, Y. Du, G. Huang, and T. Sampe, 2009: Indian Ocean capacitor effect on Indo–western Pacific climate during the summer following El Niño. *J. Climate*, **22**, 730–747, <https://doi.org/10.1175/2008JCLI2544.1>.
- Xu, W. F., L. J. Ma, M. N. Ma, H. C. Zhang, and W. P. Yuan, 2017: Spatial-temporal variability of snow cover and depth in the Qinghai-Tibetan Plateau. *J. Climate*, **30**, 1521–1533, <https://doi.org/10.1175/JCLI-D-15-0732.1>.
- Xue, Y. K., and Coauthors, 2018: Spring land surface and subsurface temperature anomalies and subsequent downstream late spring–summer droughts/floods in North America and East Asia. *J. Geophys. Res.: Atmos.*, **123**, 5001–5019, <https://doi.org/10.1029/2017jd028246>.
- Yu, S. H., W. L. Gao, and J. Peng, 2015: Circulation features of sustained departure Plateau vortex at middle tropospheric level. *Plateau Meteorology*, **34**, 1540–1555, <https://doi.org/10.7522/j.issn.1000-0534.2014.00134>. (in Chinese with English abstract)
- Zhang, R. H., A. Sumi, and M. Kimoto, 1999: A diagnostic study of the impact of El Niño on the precipitation in China. *Adv. Atmos. Sci.*, **16**, 229–241, <https://doi.org/10.1007/BF02973084>.
- Zhang, S. B., L. X. Meng, Y. Zhao, X. Y. Yang, and A. N. Huang, 2022: The influence of the Tibetan Plateau monsoon on summer precipitation in central Asia. *Frontiers in Earth Science*, **10**, 771104, <https://doi.org/10.3389/feart.2022.771104>.
- Zhao, P., Z. J. Zhou, and J. P. Liu, 2007a: Variability of Tibetan spring snow and its associations with the hemispheric extratropical circulation and East Asian summer monsoon rainfall: An observational investigation. *J. Climate*, **20**(15), 3942–3955, <https://doi.org/10.1175/JCLI4205.1>.
- Zhao, P., Y. N. Zhu, and R. H. Zhang, 2007b: An Asian-Pacific teleconnection in summer tropospheric temperature and associated Asian climate variability. *Climate Dyn.*, **29**, 293–303, <https://doi.org/10.1007/s00382-007-0236-y>.
- Zhao, Y., X. J. Yu, J. Q. Yao, X. N. Dong, and H. J. Li, 2019: The concurrent effects of the South Asian monsoon and the plateau monsoon over the Tibetan Plateau on summer rainfall in the Tarim Basin of China. *International Journal of Climatology*, **39**, 74–88, <https://doi.org/10.1002/joc.5783>.
- Zong, Y. Q., and X. Q. Chen, 2000: The 1998 Flood on the Yangtze, China. *Natural Hazards*, **22**(2), 165–184, <https://doi.org/10.1023/A:1008119805106>.